THE JOURNAL OF PHYSICAL CHEMISTRY B

Article

pubs.acs.org/JPCB

Quantum-Mechanical Study on the Aquaions and Hydrolyzed Species of Po(IV), Te(IV), and Bi(III) in Water

Regla Ayala,[†] José Manuel Martínez,[‡] Rafael R. Pappalardo,[‡] and Enrique Sánchez Marcos*[,‡]

[†]Department of Inorganic Chemistry, CSIC, ICMSE, and [‡]Department of Physical Chemistry, University of Seville, Seville 41012, Spain

Supporting Information

ABSTRACT: A systematic study of $[M(H_2O)_n(OH)_m]^{q+}$ complexes of Te(IV) and Bi(III) in solution has been undertaken by means of quantum mechanical calculations. The results have been compared with previous information obtained for the same type of Po(IV) complexes (*J. Phys. Chem. B* **2009**, *113*, 487) to get insight into the similarities and differences among them from a theoretical view. The evolution of the coordination number ($n + m$) with the degree of hydrolysis (m) for the stable species shows a systematic decrease regardless the ion. A general behavior on the M−O distances when passing from the gas phase to solution, represented by the polarizable continuum model (PCM), is also observed: R_{M-O} values corresponding to water molecules decrease, while those of the hydroxyl groups slightly increase. The hydration numbers of aquaions are between 8 and 9 for the three cations, whereas hydrolyzed species behave differently for Te(IV) and Po(IV) than for Bi(III), which shows a stronger trend to dehydrate with the hydrolysis. On the basis of the semicontinuum solvation model, the hydration Gibbs energies are −800 (exptl −834 kcal/mol), −1580 and −1490 kcal/mol for Bi(III), Te(IV), and Po(IV), respectively. Wave function analysis of M−O and O−H bonds along the complexes has been carried out by means of quantum theory of atoms in molecule (QTAIM). Values of electron density and its Laplacian at bond critical points show different behaviors among the cations in aquaions. An interesting conclusion of the QTAIM analysis is that the prospection of the water O−H bond is more sensitive than the M−O bond to the ion interaction. A global comparison of cation properties in solution supplies a picture where the Po(IV) behavior is between those of Te(IV) and Bi(III), but closer to the first one.

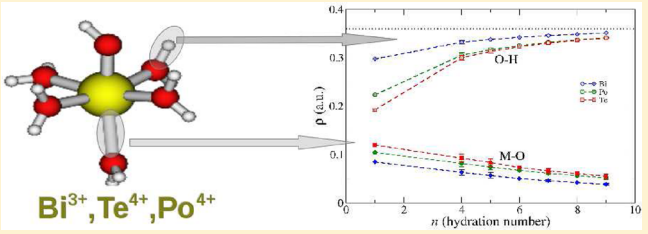

INTRODUCTION

In spite of the fact that ion solvation has long been studied,[1−4] the treatment of ion−solvent interactions still remains a central problem in the physical chemistry of electrolyte solutions. Fundamental aspects of the solution chemistry of heavy-metal ions remain unknown, even though they have important environmental consequences due to their high chemical toxicity and in some cases, also their radio toxicity. A historically relevant case is that of the polonium ion in aqueous solution; the coordination number and the hydration enthalpy of this ion have not been yet experimentally determined due to its rareness in Nature, difficult synthesis, and extreme toxicity.[5,6] To get insight into this topic, we have focused on the theoretical description of polonium(IV) hydration using quantum chemical methods and ab initio molecular dynamics simulations.[7−9] Our results showed that under the acidity conditions of our model, the coordination number of Po(IV) in aqueous solution is 6, due to an equilibrium between the $[Po(H_2O)_4(OH)_2]^{2+}$ and $[Po(H_2O)_3(OH)_3]^{+}$ hydroxy-aquaions. It was also found that the Po(IV) coordination number significantly decreases as the hydrolysis reaction proceeds. The dynamic description supplied by the ab initio molecular dynamics simulations[9] allowed us to gain insight into the reaction mechanism for the stabilization of the Po(IV) aquaion. This study reveals a stepwise mechanism in which dehydration steps follows hydrolysis, which allowed us to provide a picture about Po(IV) aqueous solutions.

At the time of the polonium discovery there was a controversy on whether the new element chemistry was more similar to that of bismuth or tellurium.[10] Although this uncertainty was resolved when polonium was assigned to group VI of the periodic table underneath tellurium, there has not yet been a comparative theoretical study of their solution chemistry. We face this issue from a quantum mechanical perspective providing a comparative study among Po(IV), Te(IV), and Bi(III) in water.

Contrary to Po(IV), Bi(III) aqueous solutions have been widely studied due to the different roles played by bismuth ion in biological and chemical systems.[11] The simple monomeric aquaion, $[Bi(H_2O)_n]^{q+}$, was characterized from acidic solutions as a triflate salt. A hydration number between 6 and 9 has been reported in its first shell.[3,4,12−17] Hydrolyzed species containing only one Bi(III) ion have been identified from 10^{-5} M solutions.[2,18] These species are in equilibrium with each other as shown in the following equation:

Received: September 22, 2012
Revised: November 26, 2012
Published: November 29, 2012

Scheme 1. Thermodynamical Cycle That Shows the Solvation Process of $[M(H_2O)_n(OH)_m]^{q-m}$ Clusters (M Being Te or Bi and p = 4 or 3, Respectively, n = 0−9 and m = 0−4 for Te and m = 0−3 for Bi)

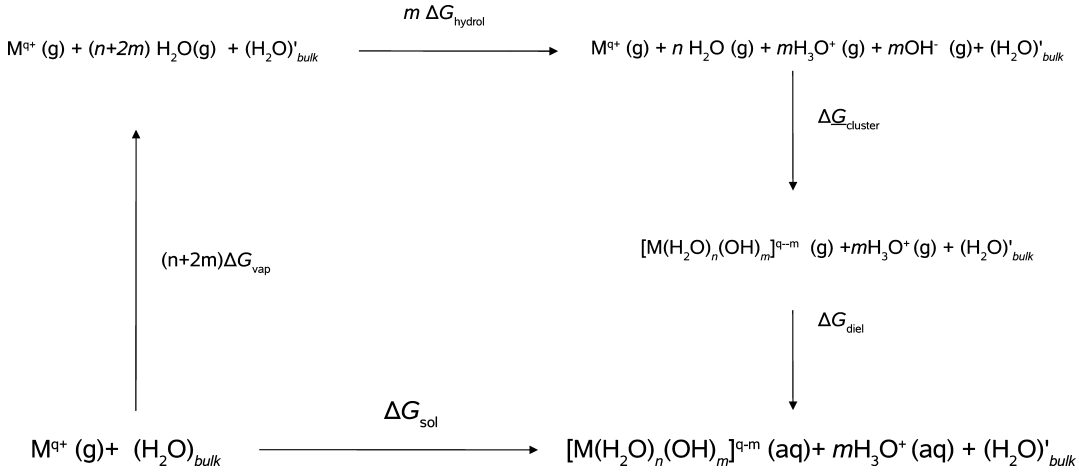

$$[Bi(H_2O)_n]^{3+} \overset{pH<3}{\rightleftharpoons} [Bi(H_2O)_{n-1}(OH)]^{2+} \overset{pH=0-4}{\rightleftharpoons} [Bi(H_2O)_{n-2}(OH)_2]^{+} \overset{pH=1-5}{\rightleftharpoons} [Bi(H_2O)_{n-3}(OH)_3] \overset{pH>11}{\rightleftharpoons} [Bi(H_2O)_{n-4}(OH)_4]^{-}$$

The mononuclear species are present in detectable quantity only in dilute solutions. In concentrated solutions (above 0.1 M), the Bi(III) aquaion is present in strongly acid solution (pH $\leq$ 0), whereas the $[Bi(OH)_4]^-$ anionic form appears in strongly basic solutions (pH $\geq$ 14). In the intermediate range, polynuclear species seem to be stable,[2] hexameric bismuthyl oxo-hydroxy species such as $[Bi_6O_4(OH)_4]^{6+}$ are the prevalent ones in solution.

In the case of the tellurium ion, strong evidence for the formation of Te(IV) ion comes from measurements of the TeO_2 in acidic solutions.[19] The aquaion $[Te(H_2O)_n]^{4+}$ has not been identified in solution so far. Whether the ion should be represented as $[Te(OH)_3]^+$, $[TeO(OH)]^+$, or $HTeO_2^+$ is even unclear. Speciation of Te(IV) in water shows that $[Te(OH)_3]^+$ is the most abundant form in dilute ($<10^{-3}$ M) solutions at pH < 2, but $[TeO(OH)]^+$ becomes dominant for pH > 4, whereas at pH > 8 the prevalent form is $[TeO_2(OH)_2]^{2-}$. $[Te(OH)_4]$ appears to reach a maximum (≡13% of the total tellurium) at pH ∼ 3.[2]

To compare Po(IV) to Te(IV) and Bi(III) in aqueous solution, we have used structural, bonding, and energetics criteria based on quantum chemical calculations in the gas phase and in solution considering aquaions and hydrolyzed species $[M(H_2O)_n(OH)_m]^{q+}$. The study intends to compare the behavior of the three cations on the same foot, and to extract the most significant similarities and differences among them.

METHODOLOGY

Geometry optimizations of $[Te(H_2O)_n(OH)_m]^{4-m}$ (n = 0−9, m = 0−4) and $[Bi(H_2O)_n(OH)_m]^{3-m}$ (n = 0−9, m = 0−3) clusters in the gas phase and in solution were performed with the Gaussian03 program.[20] Second energy derivatives on all optimized structures were carried out to check that only real frequencies were observed. On the basis of our previous Po(IV) aquaion results,[7,8] the MPW1PW91 functional[21] was used together with the Dunning aug-cc-pVDZ[22] basis sets for O and H. For Te and Bi, the aug-cc-pVDZ-PP relativistic core pseudopotentials developed by Dolg and co-workers[23,24] were used for the core electrons while the valence electrons were described with the aug-cc-pVDZ basis set.[24,25] Although the choice of the computational level for Po was already justified in previous works,[7,8] it is worth checking its performance with the two new cations. For that purpose, calculations involving larger basis sets and/or different computational strategies have been performed. Figure S1 in the Supporting Information presents the evolution of the interaction energy per water molecule for several Bi(III), Te(IV) and Po(IV) aquaions, $[M(H_2O)_n]^{q+}$ (n = 1−8). DFT-B3LYP, MP2, and CCSD(T) results are compared with those derived from the chosen MPW1PW91 functional, using in all cases the aug-cc-pVDZ basis sets. It is shown that differences are rather small, in particular when the hydration number approaches values of the stable species in solution. Interestingly, the uncertainty joined to the computational level is much smaller than the gap among the three cations. This gives us confidence in the unbiassed comparative analysis further developed. Table S1 (Supporting Information) compares the M−O distance for several aquaions obtained with the above indicated methods. The R_{M-O} behavior is similar to that observed for the interaction energy: distances differ by a few hundreths of angströms, becoming 0.01 Å for the larger hydrates (n = 6 and 8).

Concerning the basis sets quality, the Bi(III) and Te(IV) hexahydrates have been optimized additionally at the MPW1PW91 level with the aug-cc-pVTZ basis sets. R_{M-O} distances differ in 0.01 Å with respect to the values obtained when using the basis employed for the rest of calculations (aug-cc-pVDZ). Regarding the impact of the basis sets on the interaction energy of the hexahydrates, for Te(IV) it changes from −904.5 kcal/mol (DZ-type) to −908.4 kcal/mol (TZ-type), and for Bi(III) from −460.7 kcal/mol (DZ-type) to −464.1 kcal/mol (TZ-type).

The basis set superposition error (BSSE) of the formation energy of the cluster was not considered due to its small contribution at the computational level here employed. Typically BSSE correction is about 0.4%, and even smaller when dealing with reaction energy values due to a partial mutual cancellation.Thus, the BSSE correction is 0.3 kcal/mol for the hydration step $[Po(H_2O)]^{4+} + H_2O \rightarrow [Po(H_2O)_2]^{4+}$. Similar

dx.doi.org/10.1021/jp309439f | J. Phys. Chem. B 2012, 116, 14903−14914

Table 1. M−O Distances (Å) of the $[M(H_2O)_n]^{q+}$ Clusters in the Gas Phase (M Being Te, Po, or Bi, n = 4−9 for Te and Po, n = 3−9 for Bi, q = 4 for Te and Po, and q = 3 for Bi) Optimized at the MPW1PW91 Level[a]

n,m	$R_{Te-O(H_2O)}$	ΔR_{sol}	$R_{Po-O(H_2O)}$	ΔR_{sol}	$R_{Bi-O(H_2O)}$	ΔR_{sol}
3,0					2.24 × 3	−0.04
4,0	2.06 × 2	−0.06	2.17	−0.08	2.24	−0.04
	2.16 × 2	−0.15	2.18	−0.07	2.26	−0.05
			2.26 × 2	−0.03	2.36 × 2	−0.04
5,0	2.06	−0.04	2.17	−0.07	2.25	−0.04
	2.18	−0.08	2.28 × 4	−0.08 × 2	2.38 × 4	−0.07 × 2
	2.20 × 2	−0.06		−0.06 × 2		−0.04 × 2
6,0	2.24 × 6	−0.06	2.31 × 6	−0.06	2.42 × 6	−0.04
7,0	2.25 × 3	−0.07 × 2	2.33 × 2	−0.06	2.43 × 3	−0.05
		−0.04				−0.04 × 2
	2.29 × 2	−0.07	2.36 × 2	−0.11	2.47 × 2	−0.06
		−0.06		−0.07		
	2.34 × 2	−0.04	2.37	−0.07	2.49 × 2	−0.05
			2.38 × 2	−0.07		
				−0.06		
8,0	2.32 × 8	−0.05	2.38 × 8	−0.05 × 8	2.49 × 8	−0.06
9,0	2.34 × 6	−0.06 × 3	2.40 × 6	−0.05 × 2	2.52 × 6	−0.04 × 3
		−0.05 × 3		−0.04 × 4		−0.03 × 3
	2.44 × 3	−0.08	2.46 × 3	−0.08 × 2	2.56 × 3	−0.05
				−0.06		

[a] $\Delta R_{sol} = R_{M-O}(\text{solution}) - R_{M-O}(\text{gas phase})$, means the change inM-O distance due to solvent effects.

conclusions are found by Kerridge and Kaltsoyannis examining the Sr^{2+} hydration.[26]

Solvent effects on the metal cation clusters were treated on the basis of a continuum-discrete model.[27−29] This semicontinuum model considers a cavity containing the solute and its first solvation shell inmersed in a polarizable dielectric continuum. The polarizable continuum model (PCM) approach was used for the continuum cavity model.[30,31] The relative dielectric permittivity of liquid water at 25 °C (ε = 78.39) was used for the dielectric medium. The gas-phase geometries were fully reoptimized using the PCM model to take account of the nuclear relaxation of the clusters induced by solvent effects. Cavities were built on the basis of a set of interlocking spheres, for which the following atomic radii were employed: 1.52 Å for O, 1.20 Å for H, and 2.24 and 2.19 Å for Te and Bi, respectively.[32,33] The radii have been multiplied by a standard factor of 1.2 to take into account the fact that atomic bond or lone pair centers of the solvent molecules are normally located slightly further away from the solute atoms than van der Waals radius.[30]

As shown in a number of previous studies on monatomic cation hydration, the explicit consideration of solvent molecules to describe the first hydration shell is necessary to achieve reliable values of solvation free energies.[28,34] Inclusion of the second or outer solvation shells is not generally used due to the rapid increase of computational effort and due to methodological concerns associated to the lack of a proper inclusion of statistical contributions in the quantum mechanical computations.[34,35]

A Gibbs energy in solution, ΔG_{sol}, can be defined for a given hydrated/hydrolyzed form of Te(IV) and Bi(III) within the semicontinuum model[27,35,31] following the thermodynamical cycle shown in Scheme 1, where $(H_2O)_{bulk}$ means pure water and $(H_2O)'_{bulk}$ denotes pure water without the appropriate number of water molecules that have been released from the bulk to form a given cluster.[8] From Scheme 1, the following relationship is obtained:

$$\Delta G_{sol} = (n + 2m)\Delta G_{vap} + m\Delta G_{hydrol} + \Delta G_{cluster} + \Delta G_{diel} \quad (1)$$

where $(n + 2m)\Delta G_{vap}$ is the free energy needed to evaporate $(n + 2m)$ molecules from liquid water to the gas phase; $m\Delta G_{hydrol}$ is the free energy necessary to hydrolyze $2m$ water molecules into OH^- and H_3O^+ fragments; $\Delta G_{cluster}$ is the free energy of formation of the cluster; ΔG_{diel} is the solvation free energy associated to the process of including the corresponding species inside of a cavity immersed in a continuum. ΔG_{diel} is decomposed into three contributions $\Delta G_{cav} + \Delta G_{disp-rep} + \Delta G_{cont}$, where ΔG_{cav} is the free energy needed to create the cavity, $\Delta G_{disp-rep}$ collects the solute-continuum dispersion and repulsion contributions, and ΔG_{cont} is the solvation energy corresponding to the long-range interactions of the hydrated cluster in the cavity embedded in the polarizable continuum.[30,31] A temperature of 298 K was assumed for the computation of the thermodynamic properties.

A proper calculation of ΔG_{sol} needs an additional term that accounts for the different thermodynamic state of water molecules in the gas phase and in solution of Scheme 1.[34,36−38] Experimental and calculated gas-phase free energies are often defined by assuming the standard state as that of an ideal gas at 1 atm, whereas free energies of solvation are associated with the 1 M (gas) → 1 M (solution) process. However, the concentration of water in liquid water is 55.5 M, yielding a pressure of 1356 atm (from $P = \rho RT$). Each water molecule has less translational freedom, as the translational entropy partition function is pressure dependent. The result is a lowering of the overall solvation free energy of reaction of −4.3 kcal/mol per water molecule evaporated from the bulk.[34,36−38]

According to that, Goddard and co-workers[38] derived an approach for predicting the solvation free energies of charged solutes using a semicontinuum model of solvation. Their proposed scheme is pretty close to ours when computing ΔG_{sol} for aquaions.[8] Nevertheless, they consider water clusters $((H_2O)_n)$ instead of the independent water molecules

Table 2. M−O Distances (Å) of the $[M(H_2O)_n(OH)_m]^{q-m}$ Clusters (M Being Te and Po, −-7, m = 1−4, and q = 4 and M Being Bi n = 0−6, m = 1−3, and q = 3) Optimized at the MPW1PW91 Level in the Gas Phase[a]

n,m	$R_{Te-O(H_2O)}$	ΔR_{sol}	$R_{Te-O(OH)}$	ΔR_{sol}	$R_{Po-O(H_2O)}$	ΔR_{sol}	$R_{Po-O(OH)}$	ΔR_{sol}	$R_{Bi-O(H_2O)}$	ΔR_{sol}	$R_{Bi-O(OH)}$	ΔR_{sol}
2,1									2.26	−0.04	2.00	0.02
									2.28	−0.04		
3,1	2.11	−0.04	1.86	0.00	2.22	−0.05	1.96	0.00	2.30	−0.02	2.01	0.02
	2.16	−0.06			2.25	−0.04			2.37	−0.04		
	2.20	−0.05			2.30	−0.07			2.42	−0.05		
4,1	2.17	−0.03	1.87	0.01	2.27	−0.04	1.97	0.01	2.37	0.00	2.03	0.02
	2.22 × 2	−0.05			2.31 × 3	−0.05			2.43 × 2	−0.04		
	2.24	−0.05							2.44	−0.05		
5,1	2.25	−0.02	1.88	0.00	2.27	−0.01	2.00	0.00	2.46 × 2	−0.03	2.03	0.03
										−0.02		
	2.28	−0.03			2.30	−0.04			2.47	−0.02		
	2.29	−0.04			2.36	−0.05			2.52	−0.06		
	2.34	−0.05			2.59	−0.09			2.57	−0.08		
6,1[b]	2.20		1.90		2.35	−0.05	2.00	0.01				
	2.21				2.36	−0.05						
	2.25				2.37	−0.03						
	2.31				2.39	−0.03						
	2.35				2.45	−0.06						
	2.69				2.63	−0.07						
7,1[b]	2.26 × 2		1.91		2.36	−0.02	2.01	0.03				
	2.27				2.38 × 2	−0.04						
	2.29					−0.02						
	2.30				2.41 × 2	−0.05						
	2.67					−0.04						
	2.72				2.63	−0.07						
					2.71	−0.12						
2, 2	2.24 × 2	−0.04	1.88	0.01	2.34 × 2	−0.04	1.98	0.01	2.47 × 2	−0.03	2.04	0.02
			1.89	0.00			1.99	0.01			2.06	0.01
3,2	2.28 × 2	−0.05	1.89	0.01	2.36	−0.04	1.99	0.01	2.48	−0.02	2.05	0.02
	2.57	−0.09	1.90	0.01	2.37	−0.05	2.00	0.02	2.49	−0.03	2.06	0.02
					2.60	−0.1.			2.91	−0.14		
4,2[b]	2.20		1.92 × 2		2.33	−0.02	2.01	0.02	2.48		2.09	
	2.30				2.41	−0.04	2.02	0.01	2.49		2.10	
	2.55				2.59	−0.05			2.74			
	2.58				2.65	−0.09			2.85			
5,2[b]	2.24 × 2		1.92		2.36 × 2	−0.01	2.02	0.02	2.48 × 2		2.10 × 2	
	2.58 × 2				2.65	−0.06	2.03	0.02	2.83			
	2.59				2.70	−0.10			3.03 × 2			
					2.80	−0.19						
2,3	2.57	−0.08	1.93 × 2	0.00	2.57	−0.04	2.03	0.01	2.68	0.06	2.10	0.00
	2.58	−0.03		0.01	2.58	−0.05	2.04	0.02	2.83	0.05	2.14	0.01
							2.05	0.01			2.15	0.00
3,3	2.60 × 3	−0.03	1.95 × 3	0.01	2.62 × 3	−0.05	2.05 × 3	0.01	2.74	0.05	2.10	0.00
		−0.02 × 2				−0.03 × 2			2.80	0.03	2.14	0.00
									2.94	−0.03	2.18	0.00
0,4			1.95 × 2	0.00			2.05 × 2	0.00				
			1.98	0.03			2.13	0.01				
			2.08	−0.02			2.19	−0.01				
1,4	2.88	0.21	1.95 × 2	0.00	2.76	−0.02	2.05 × 2	0.00				
			2.03	0.02			2.13	0.01				
			2.09	0.00			2.19	−0.01				

[a] ΔR_{sol} gives the change in M−O distance due to solvent effects (see Table 1 for definition). [b] The clusters without ΔR_{sol} information were only optimized in solution because they were not stable in the gas phase.

$(n(H_2O))$ in the computation of ΔG_{vap} and $\Delta G_{cluster}$. These authors propose that taking into account water clusters a systematic error presented in the solvation due to hydrogen-bonded interactions is avoided. The underlining assumption behind this approach is that the interactions between hydrated charged species and bulk water are similar to those between $(H_2O)_n$ and bulk water in the limit of large n. In the present work, the computation of ΔG_{sol} for aquaions was carried out using both methods, that proposed in Scheme 1 and Goddard et al.'s approach.[38] ΔG_{sol} computation for hydrolyzed species using

dx.doi.org/10.1021/jp309439f | J. Phys. Chem. B 2012, 116, 14903−14914

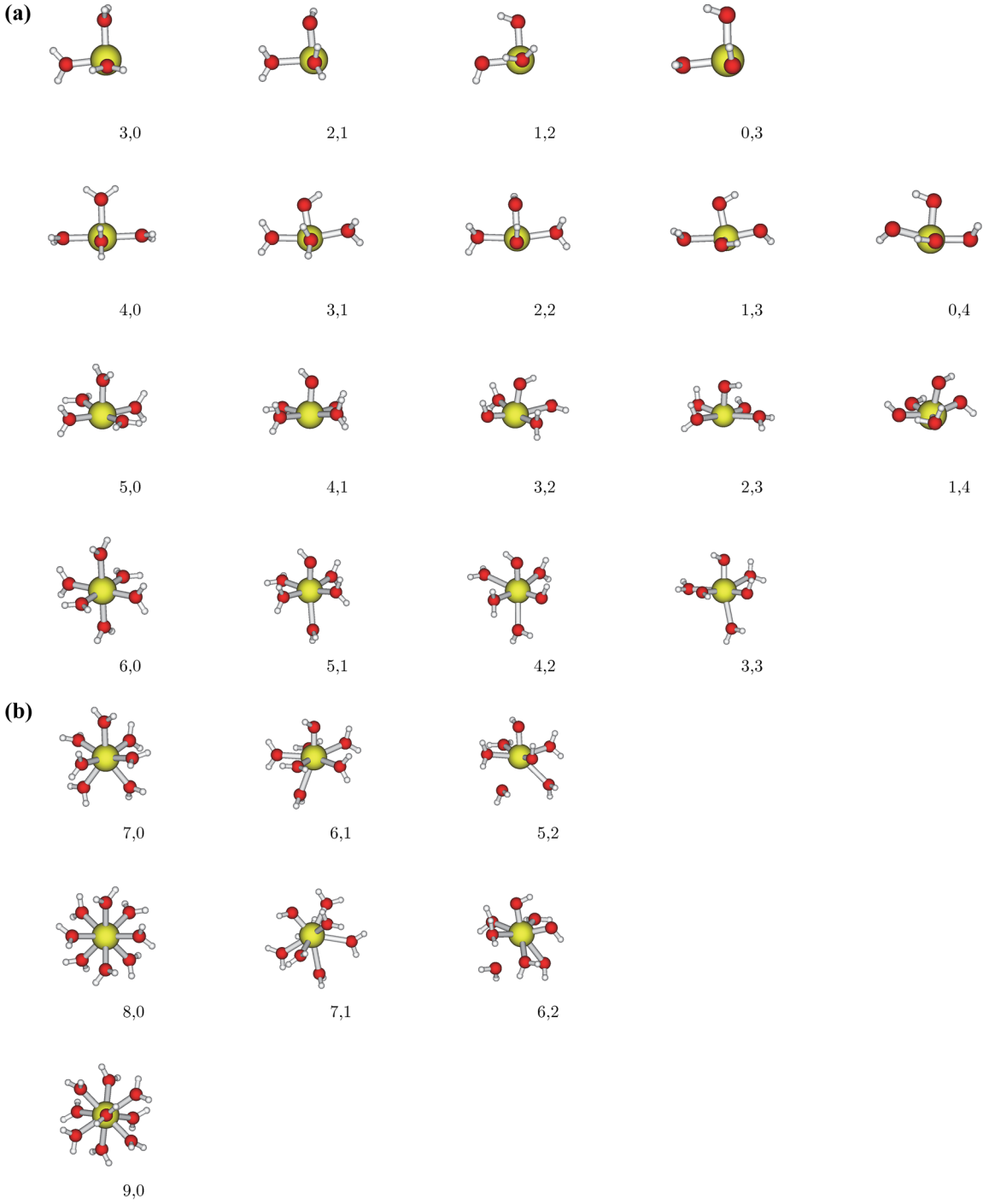

Figure 1. Representative model structures for $[M(H_2O)_n(OH)_m]^{q-m}$ clusters with M being Te, Po, and Bi, n = 3−9 and m = 0−4.

Goddard's strategy was not possible because no metal−H_2O aggregates with more than nine water molecules in its first solvation shell were found. The addition of a tenth water molecules gives rise to $[M(H_2O)_8(OH)]^{q-1}$ + H_3O^+. This process can not be avoided without constrains.

The topology of the electron density (ρ) and its laplacian ($\nabla^2\rho$) were studied within the framework of the quantum theory of atoms in molecules (QTAIM) method[39,40] as implemented in the AIMALL program.[41] The checkpoint files produced by Gaussian03 program were read in the Gaussian09[42] program to create the ".wfx" type file used by AIMALL. This step was needed due to the use of RECP in our calculations. In this way a set of atomic core cluster densities are used to model the core electrons and avoid the appearance of spurious critical points.[43] The reported ρ and $\nabla^2\rho$ values correspond to electron densities computed in the gas phase. A few comparisons between ρ values obtained from the gas phase and in solution revealed a marginal effect of the dielectric continuum on the bond critical points at the same geometrical structure.

RESULTS AND DISCUSSION

Structural Properties. Tables 1 and 2 collect Te−O and Bi−O distances for aquaions and hydrolyzed species optimized in the gas phase and the change of these distances when solvent

dx.doi.org/10.1021/jp309439f | J. Phys. Chem. B 2012, 116, 14903−14914

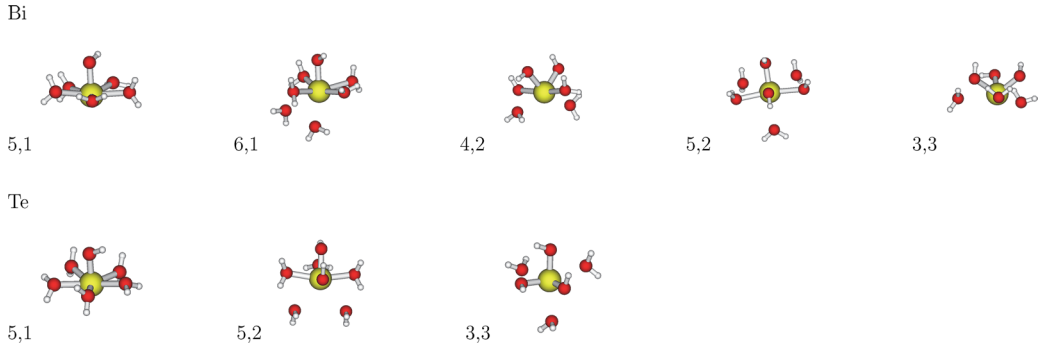

Figure 2. MPW1PW91 optimized structures in solution using a semicontinuum model for $[Bi(H_2O]_5(OH)]^{+2}$, $[Bi(H_2O]_6(OH)]^{+2}$, $[Bi(H_2O]_4(OH)_2]^{+}$, $[Bi(H_2O]_5(OH)_2]^{+}$, $[Bi(H_2O]_3(OH)_3]$, $[Te(H_2O]_5(OH)]^{+3}$, $[Te(H_2O]_5(OH)_2]^{2+}$, and $[Te(H_2O]_3(OH)_3]^{+}$ clusters.

effects are considered ($\Delta R_{sol} = R_{solution} - R_{gas-phase}$). For the sake of comparison, our previous results[7,8] for the Po(IV) ion have also been included.

As expected, the metal−oxygen distances increase with the number of ligands contained in the aggregate for aquaions and hydrolyzed species. Following the sequence Te → Po → Bi the metal−oxygen distances also increase. The analysis of tables indicates that M−O(H_2O) distances shorten ($\Delta R_{sol} < 0$) when going from the gas phase to solution for aquaions (Table 1) and the same trend is observed for the hydrolyzed species (Table 2). On the contrary a slight lengthening of the M−O(OH) distances ($\Delta R_{sol} > 0$) is caused by solvent effects (Table 2). It must be mentioned that some exceptions from this general behavior can be found for the most hydrolyzed species of the Te(IV), Po(IV), and Bi(III) ions. In these cases the water molecules are pretty far from the ion and to a certain extent they can be considered located in between the first and the second solvation shells.

Most of the $[M(H_2O)_n(OH)_m]^{q-m}$ clusters optimized in the gas phase and in solution present similar structures regardless the nature of the ion. For this reason, Figure 1 collects common arrangements of ligands around the ion and can be considered representative of the structure for Te(IV), Po(IV) and Bi(III) clusters. It is important to note that not all the clusters included in Figure 1 are minima in the Te(IV) and Bi(III) potential energy surfaces. Only those clusters whose distances have been collected in Tables 1 and 2 are optimized in the gas phase and/or solution. They were characterized as true minima by checking that all their frequencies are real. Additional prospections of possible conformers by rotation of the hydroxyl groups lead to the conclusion that alternant orientations of OH groups, as seen in structures (1,2) or (2,2) of Figure 1 are the preferred geometries.

The analysis of Figure 1 indicates that clusters up to five water molecules must be considered as surface clusters, i.e., that the ion is not completely embedded in the cluster. This arrangement can be explained in terms of an orbital contribution to the ion−ligand bonding based on the interaction between the valence p orbitals of ion and the lone pairs of water molecules, the role of the valence s orbital of metal ion being negligible. Nevertheless, for larger clusters containing up to nine water molecules, the ligand arrangement places the ion inside the clusters surrounded by symmetrically distributed water molecules (the arrangement of the water molecules was detailed in ref 8).

A common trend for hydrolyzed clusters, already observed in the polonium ion,[8] is the fact that water molecules in trans positions with respect to OH^- ligands are located at longer distances from the metal ion than the other water molecules in the cluster (see, e.g., M−O distances in (6,1) cluster in Table 2). This fact is explained as a trans-effect,[44,45] induced by hydroxyl groups on the water molecules in trans position with respect to them. Additionally, the water molecule trans to the OH^- ligand deviates from the direction described by the metal ion−O(OH) vector by 30−60°. This feature is well-identified when there is only one hydroxyl ligand in the cluster. However, it is more difficult to observe when the number of OH^- increases because the final arrangement becomes a compromise among several factors such as electrostatic interactions and steric repulsions.

When two or three OH^- ligands are present in a cluster, the adopted arrangement is such that hydroxyl ligands avoid each other to be opposite. Thus, clusters with two OH^- ligands (e.g., structures (2,2), (3,2) and (4,2) in Figure 1) have the OH^- groups mutually orthogonal. A similar rule is followed when three OH^- ligands are present (e.g., structures (1,3) and (2,3) in Figure 1). Two OH^- groups opposite to each other are found in clusters with four OH^- ligands (structures (0,4) and (1,4) in Figure 1). When two OH^- ligands are in a trans position, metal−O distances are longer than those for the other OH^- groups.

Although there are many common features among the $[M(H_2O)(OH)_m]^{q-m}$ clusters for Po(IV), Te(IV), and Bi(III) ions, some clusters, especially in the case of the Bi(III) ion, present noticeable differences that deserve a separate comment. These clusters are displayed in Figure 2. It is worth pointing out that most of the aggregates in Figure 2 are not stable in the gas phase, in the sense that some of the water molecules are expelled to the second hydration shell giving rise to hydrolysis events. Thus, they were only optimized in solution.

In the case of $[Bi(H_2O)_5OH]^{2+}$ and $[Te(H_2O)_5OH]^{3+}$ aggregates, the five water molecules and the ion are contained in a plane whereas the hydroxyl group is in an axial position, that is, they present a distorted pentagonal pyramid geometry. The analogous cluster for the polonium ion (clusters (5,1) in Figure 1) presents a distorted octahedral geometry very similar to that of the $[M(H_2O)_6]^{q+}$ aggregates. A minimum structure where all the water molecules are in the same plane can be obtained for the polonium ion; however, this structure is less stable than cluster (5,1) in Figure 1. $[Bi(H_2O)_5OH]^{2+}$ and $[Te(H_2O)_5OH]^{3+}$ clusters in a distorted octahedral geometry (like cluster (5,1) in Figure 1) are not minima in their corresponding potential energy surfaces and the water molecule, initially in a trans position to the hydroxyl group, migrates to the equatorial plane yielding a pentagonal pyramid structure.

Except for the $[Bi(H_2O)_5OH]^{2+}$ and $[Te(H_2O)_5OH]^{3+}$ aggregates, the remaining clusters in Figure 2 present at least

two water molecules that can be considered between the first and second solvation shells. This means that they are simultaneously interacting with the ion and with other water molecules in the cluster. This is illustrated by the long M–O(H_2O) distances collected in Table 2 and the peculiar orientations of these water molecules with respect to the ion.

Free Energies. Free energies in solution, ΔG_{sol}, for the different Te(IV) and Bi(III) clusters are shown in Figures 3 and

n+m \ m	0	1	2	3	4
4	-1496.7 (-1499.7)	-1481.3	-1439.6	-1371.4	**-1273.2**
5	-1535.3 (-1540.8)	-1508.0	-1448.6	-1374.3	-1269.3
6	-1547.9 (-1554.4)	-1514.1	-1453.5	**-1374.7**	
7	-1565.0 (-1575.6)	-1517.4	**-1454.9**		
8	**-1581.1** (-1592.6)	**-1521.1**			
9	-1575.4 (-1589.9)				

Figure 3. Free solvation energies, ΔG_{sol}, in kcal/mol, for $[Te(H_2O)_n(OH)_m]^{4-m}$ clusters (n = 4–9 and m = 0–4) computed using eq 1 for the thermodynamical cycle shown in Scheme 1. Values into parentheses are calculated by Goddard's method.[49]

n+m \ m	0	1	2	3
3	-736.2	-671.2	-593.2	**-498.5**
4	-757.9 (-761.0)	-686.8	-603.0	-497.9
5	-771.7 (-777.2)	-699.4	**-606.0**	-496.6
6	-782.1 (-788.6)	**-702.5**	-601.8	-493.2
7	-791.3 (-802.0)	-700.4	-604.8	
8	**-797.8** (-809.4)			
9	-795.6 (-810.1)			

Figure 4. Free solvation energies, ΔG_{sol}, in kcal/mol, for $[Bi(H_2O)_n(OH)_m]^{3-m}$ clusters (n = 3–9 and m = 0–3) computed using eq 1 for the thermodynamical cycle shown in Scheme 1. Values into parentheses are calculated by Goddard's method.[49]

4, respectively. For the sake of comparison, the results previously obtained for Po(IV) clusters were also included (Figure 5).[8] (ΔG_{sol} values in Figure 5 differ from those published in ref 8 because the latter do not include the thermodynamic correction commented in the Methodology section.) In these figures the row index ($n + m$) gives the total

n+m \ m	0	1	2	3	4
4	-1393.1 (-1396.1)	-1370.7	-1324.1	-1250.4	-1148.8
5	-1432.8 (-1438.2)	-1399.3	-1334.7	-1255.9	-1147.6
6	-1458.1 (-1464.6)	-1410.4	-1342.6	**-1259.4**	**-1149.7**
7	-1475.7 (-1486.4)	-1420.5	**-1347.4**	-1256.4	-1141.3
8	-1488.2 (-1499.8)	**-1424.9**	-1342.6	-1251.0	
9	**-1493.4** (-1508.0)	-1420.0	-1337.7		

Figure 5. Free solvation energies, ΔG_{sol}, in kcal/mol, for $[Po(H_2O)_n(OH)_m]^{4-m}$ clusters (n = 4–9 and m = 0–4) computed using eq 1 for the thermodynamical cycle shown in Scheme 1. Values into parentheses are calculated by Goddard's method.[49]

number of ligands bonded to ion, whereas the column index (m) gives the total number of OH^- groups in the cluster. Within a row, a move from left to right formally implies an increase in the basicity of the medium as more hydrolyzed species are obtained. On the contrary, the degree of hydrolysis is constant along a column, the difference among species being the number of water molecules in the cluster, that is the hydration degree. In this case, the stability results must be interpreted on the basis of a constant degree of acidity/basicity in the medium. Thus, meaningful comparisons can only be done among species within a column because the differences arise only from the number of water molecules released from the infinite solvent bath to the cluster without any formal change in the chemical nature of the solute. The most negative value for each degree of hydrolysis has been bolded. However, it may be observed that the differences among ΔG_{sol} values for the most stable clusters are frequently small enough to consider an equilibrium between different species rather than the existence of only one hydrated form. The holes appearing in Figures 3 and 5 are due to the impossibility of optimizing metal–ligand aggregates neither in the gas phase nor in solution for the corresponding coordination. It is worth pointing out that the number of holes increases in parallel with the hydrolysis degree.

ΔG_{sol} sequences for the three cations show that the coordination number decreases as the hydrolysis proceeds. For Te(IV) the sequence of the most stable cluster for each hydrolysis degree, m, is (8,0) → (7,1) → (5,2) → (3,3) → (0,4). This reduction is similar to the case of the Po(IV) except for the most hydrolyzed cluster, which in Po(IV) case exhibits an equilibrium involving the 4, 5, and 6 ligands. The Bi(III) ion presents a steeper behavior than the tetravalent cations, its most stable cluster sequence being (8,0) → (5,1) → (3,2) → (0,3).

ΔG_{sol} values for aquaions were also computed following the scheme published by Goddard and co-workers,[38] that is, considering the vaporization of a water cluster, $(H_2O)_n$, from the bulk instead of n-times an independent water molecule ($n(H_2O)$). This procedure also implies the need to compute $\Delta G_{cluster}$ by taking into account water molecules as an aggregate. In ref 38, ΔG_{vap} and $\Delta G_{cluster}$ were computed using the most stable geometries of $((H_2O)_n)$ aggregates. We have preferred to use an alternate methodology that consists of extracting different clusters of water molecules containing between 4 and 9 water

dx.doi.org/10.1021/jp309439f | J. Phys. Chem. B 2012, 116, 14903–14914

molecules from a Monte Carlo simulation of pure water carried out in the group for other purposes, optimizing these clusters at the MPW1MPW91 level with aug-cc-pVDZ, and using them in the ΔG_{sol} computation. The final ΔG_{sol} result is the average of ΔG_{sol} obtained for each n value. Regardless of the size of the cluster, the results for the different water clusters considered in the computation hardly modifies the final value. The dispersion of values among different water clusters is between 0.1 and 6 kcal/mol, that is, just the 0.5% of the total ΔG_{sol} value. The results are shown in parentheses in Figures 3−5 for Te, Bi, and Po, respectively. They give more negative ΔG_{sol} values[38] than those obtained from Scheme 1. The experimental estimation of ΔG_{sol} is only avaliable for the Bi(III) aquaion, −834 kcal/mol.[4] The results obtained in terms of ref 38 are closer to the experimental estimations than those presented following Scheme 1 by 15 kcal/mol. However, the order of stability for the different aquaions and ions remains unchanged in both cases but for Bi(III) with n = 8 and 9. Nevertheless, this difference is small enough to consider both aquaions equally stable, as the typical uncertainty associated to the theoretical ΔG_{sol} estimation obtained by different authors on multiply charged metal cations is about 3−5%.[35−38] In the particular case of Bi(III) here studied the estimation of the hydration Gibbs energy is affected by a 3%.

The reaction free energy for the successive hydrolysis steps for a given total coordination number

$$[M(H_2O)_n(OH)_m]_{aq}^{q+} + H_2O_{aq} \rightarrow [M(H_2O)_{n-1}(OH)_{m+1}]_{aq}^{q-1} + H_3O_{aq}^{+}$$

can be calculated as the difference of the ΔG_{sol} of the species involved in the reaction. For both H_2O and H_3O^+ species, their corresponding ΔG_{sol} values were theoretically computed at the same level. A systematic compilation for the three cations and the total coordination number, $(n + m)$, from 4 to 9 has been included as Supporting Information (Tables S1(Bi), S2(Te) and S3(Po)). For a given $(n + m)$ value, the spontaneity of the step decreases with the hydrolysis degree, i.e., when m increases, and the process becomes endergonic for a given value of m. Therefore, this value may be taken as an indication of the hydrolysis process extent for each cation at a given coordination number. Figure 6 collects for the different $(n + m)$ the last equilibrium process, which is exergonic. A global comparison among the three cations indicates that the exergonic reaction extends up to a higher hydrolysis degree for Po(IV) and Te(IV) than for Bi(III). In fact, from a coordination number of 6, the Bi(III) aquaion does not present hydrolysis reactions. The comparison between Te(IV) and Po(IV) shows a slightly higher trend to hydrolysis for Te(IV) than for Po(IV). The hydrolysis degree predicted by thermochemistry shows a qualitative agreement with experimental information, as equilibrium involving $[Te(H_2O)_n(OH)_2]^{2+}$ and $[Te(H_2O)_n(OH)_2]^{+}$ species, and $[Bi(H_2O)_n]^{3+}$ and $[Bi(H_2O)_n(OH)]^{2+}$ species seem to be the most probable clusters in aqueous solution.[2,18,19]

Bonding Analysis. The quantum theory of atoms in molecule (QTAIM) offers a useful tool for the comparative analysis of the bonding properties found in the different clusters of the three cations studied. Based on the QTAIM theory,[39,40] the electron density, ρ, and its Laplacian, $\nabla^2\rho$, at a bond critical point (bcp) give us information about the strength and nature of the bond. Large ρ values together with negative values for $\nabla^2\rho$ are usually associated with covalent bonds, whereas small ρ values and positive values for $\nabla^2\rho$ are found for closed-shells and ionic interactions.[39,40] We have examined the changes of ρ and

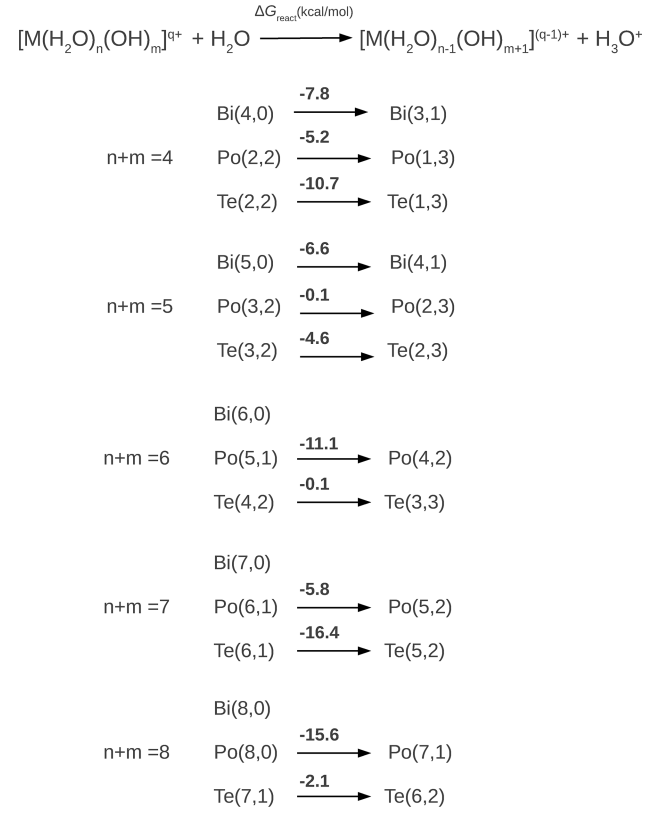

Figure 6. Free energies (kcal/mol) of hydrolysis processes, ΔG_{react}, for the $[M(H_2O)_n(OH)_m]^{q+}$ clusters of the last exothermic stepwise for each cation.

$\nabla^2\rho$ values at the bcp of the metal−oxygen bonds, M−O, which correspond either to ion−water, M−O(H_2O), or ion−hydroxyl bonds M−O(OH). Likewise, the O−H bonds of the water or hydroxyl group coordinated to the ion have been analyzed, to quantify the effect of ion−ligand interaction on the internal structure of the ligand; i.e., these points reflect the polarization and partial charge transfers occurring when a highly charged cation perturbs the covalent bonds.

Figure 7 collects the ρ(bottom) and $\nabla^2\rho$(top) values at the bcp for the M−O (Figure 7 left) and O−H (Figure 7 right) bonds for all aquaions here studied and a group of the hydrolyzed species. Apart from a very few points out of the distributions, which correspond to extreme situations, (e.g., the ρ(O−H) and $\nabla^2\rho$(O−H) values at bcp of the monohydrates, $[Te(H_2O)]^{4+}$ and $[Po(H_2O)]^{4+}$, which are the isolated red and green points with ρ values ∼0.2−0.23 au, and $\nabla^2\rho$ values of −1.5 and −1.25 au), the points are grouped in well-defined distributions. The first distribution is formed by the points corresponding to the M−O bond (Figure 7 bottom-left), which presents small ρ values (0.02−0.14 au) and decreases with R_{M-O}, i.e., when the ion−ligand interaction is weakened. There are two ρ(O−H) distributions (Figure 6 bottom-right), one for the O−H(OH^-) bonds and other for the O−H(H_2O) bonds. Both distributions present high density values denoting the covalent character of the O−H bond. It is worth noting that the ρ(O−H) value at the bcp for OH^- bonds are higher than those corresponding to the H_2O bonds for the same R_{M-O} distances (1.9−2.2 Å), which indicates that the hydroxyl group retains more covalent character than the water molecule. The two ρ(O−H) distributions show a slight increase with the distance what means that the covalent character of the O−H bond

dx.doi.org/10.1021/jp309439f | J. Phys. Chem. B 2012, 116, 14903−14914

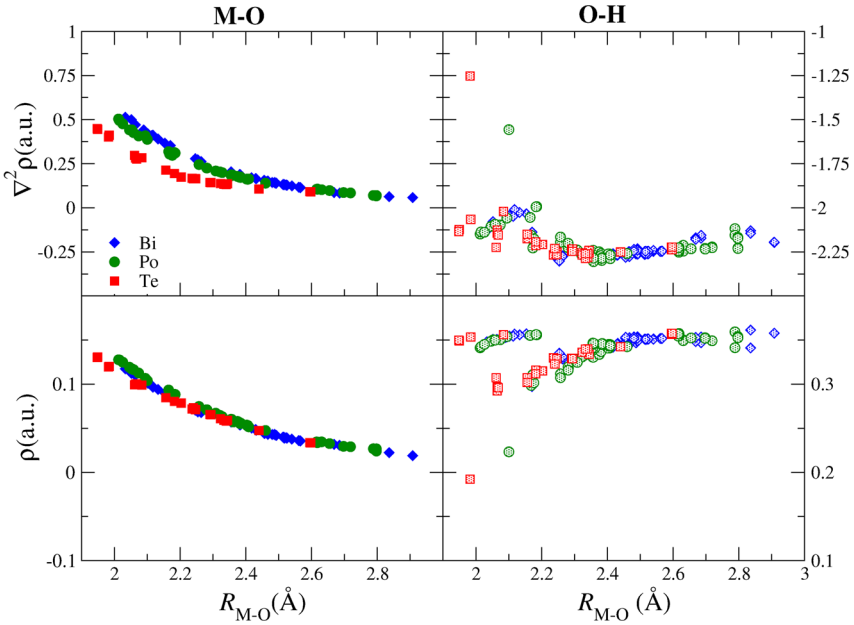

Figure 7. Electron density (bottom) and its Laplacian (top) at the bond critical point of M−O (left) and O−H (right) bonds as a function of the M−O distance.

increases with R_{M-O}. This behavior is a consequence of the recovering of the O−H bond in the ligand (H_2O or OH^-) as ion perturbation decreases with R_{M-O}. Thus, these two distributions must go up asymptotically to the ρ(O−H) values of the free H_2O (0.363 au) and O−H (0.355 au), at the calculation level employed. The subset of points at short distances (1.9−2.2 Å) and higher values (∼0.35 au) collects the hydroxyl group contributions.

A clear conclusion raising from this figure is how the electron density value at the bcp is mainly dependent on the ion−oxygen distance, regardless the cation involved or the coordination number. This is particularly clear in the case of the ρ(M−O) distribution, but it also holds up for the two ρ(O−H) distributions. In a recent study on several Sr^{2+} hydrolyzed forms, Karridge and Kaltsoyannis[46] examine the behavior of the M−O bcp, finding trends with the R_{Sr-O} similar to those here presented. This monotonic behavior is coherent with the relevance of the ionic radii in the prediction of the cation physicochemical properties, which have long been emphasized by electrochemists.[1,4,47,48] Bonding properties are strongly correlated with R_{M-O}.

The electron density Laplacian values at the same bcps are plotted in the upper part of Figure 7. As expected, large negative values (ca. −2 to −2.5 au) correspond to the O−H covalent bonds (Figure 7), whereas small negative values (ca. 0.0−0.05 au) are associated with M−O bonds (Figure 7), reflecting their ionic nature.

The global analysis of ρ and $\nabla^2\rho(r)$ at the bcps have not provided particularly significant differences among the different cations. This is in part due to the large combination of cases that may be found in the clusters examined, regarding the hydration number, the hydrolysis degree, the trans effect induced by the hydroxyl groups among them and on the opposite water molecules, etc.

To rationalize the different effects we have examined the dependency of ρ with R_{M-O} for the simplest case, i.e., the monohydrate, $[M(H_2O)]^{q+}$. This is a way to isolate the native behavior of a pure cation−water pair interaction. The curves for the M−O and O−H values are plotted in Figure 8a. The solid segments in the curves indicates the range of R_{MO} distances adopted by H_2O and OH^- ligands in all the cation complexes studied.

The three ρ(O−H) curves appear clearly separated. The ordering of the ρ(O−H) curves indicates a smaller weakening of the O−H bond in the water molecule when it interacts with Bi(III) than when it does with Po(IV) or Te(IV). For the same oxidation state the curve of Te is also departing from that of Po, which denotes a stronger perturbation of the water molecule by the lighter element. On the contrary, the ρ(M−O) curves do not show noticeable differences, the three ionic bonds increase their electron density to a similar extent when R_{M-O} is shortened. From the ρ(M−O) and ρ(O−H) values at short distances (1.9−2.1 Å) one can easily identify the very low values observed in the general plot of Figure 6, they correspond to the monohydrates.

A step beyond the effect of the ion−water distance on ρ in $[M(H_2O)]^{q+}$ is the evaluation of the many-body effects introduced by the systematic addition of water molecules in the $[M(H_2O)_n]^{q+}$ hydrate. Thus, Figure 8b plots the values for the M−O and O−H bonds as a function of the hydration number, n, for all the aquaions studied. Table 1 has shown that for some aquaions the ion−water distances are not all the same, which implies several ρ values for a given n. The plotted data are the mean values, together with their standard deviations represented by error bars. The dispersion of ρ for a given n is smaller than the gap among the curves for the different ions. The trend of the ρ(O−H) and ρ(M−O) with n is similar to that observed for the native behavior of only one water molecule with R_{M-O}. This may be understood by examining Table 1, as R_{M-O} increases with the hydration number. However, many-body effects are now a new ingredient that change qualitatively and quantitatively the electron density at the bcp. This is nicely illustrated by the ρ(M−O) curves (bottom of Figure 8b) for the different cations, which are now separated: Bi(III) curve moves apart from Te(IV) and Po(IV) curves. For the case of the ρ(O−H) curves (top of Figure 8b), that of Bi(III) exhibits a stronger

dx.doi.org/10.1021/jp309439f | J. Phys. Chem. B 2012, 116, 14903−14914

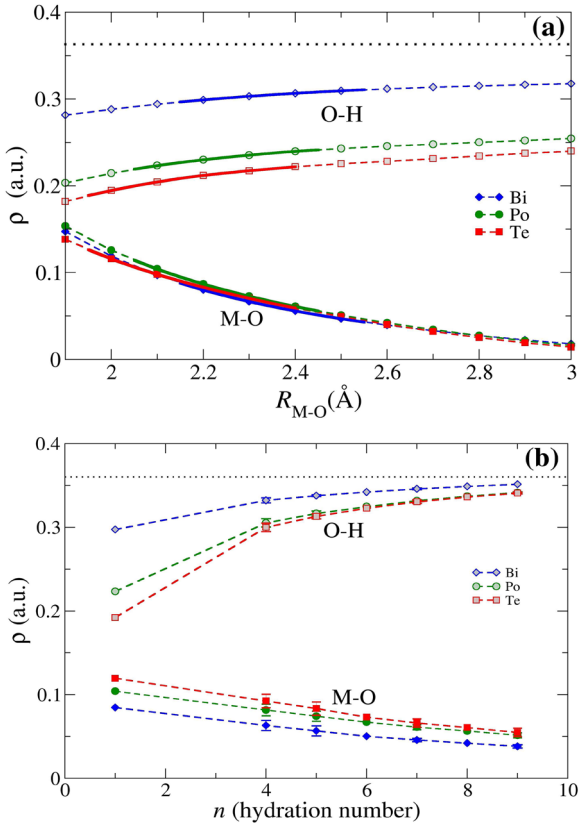

Figure 8. (a) Electron density at the bond critical point of the M−O (bottom) and O−H (top) bond for the monohydrated cations, $[M(H_2O)]^{3+/4+}$ as a function of the M−O distance. The continuous segment denotes the range of distance adopted by the clusters studied $[M(H_2O)_n(OH)_m]^{q+}$. (b) Mean electron density at the bond critical point of M−O (bottom) and O−H (top) bond for the hydrated cations, $[M(H_2O)_n]^{3+/4+}$, as a function of the hydration number.

trend to approach the limit ρ(O−H) value of a free water molecule. The increase of the hydration degree reduces the cation perturbation on each water molecule bonded to it, and consequently ρ(O−H) would increase up to reach the free water molecule value. Contrarily, ρ(M−O) would go down to 0. An interesting issue from this figure is to recognize how the many-body interactions associated with the three cations follow a different behavior, and how this behavior is different when examining the rather ionic M−O bond than the purely covalent O−H bond.

The change of the electron density values as a consequence of the successive hydration by water molecules, or in other words, by the increase of the many-body effects in the complexes can be quantified by subtracting the current ρ value for a given aquaion of the corresponding ρ value for the $[M(H_2O)]^{q+}$ curve at the mean M−O distance of the complex $\Delta\rho_{mb} = \rho_{[M(H_2O)_n]^{q+}} - \rho_{[M(H_2O)]^{q+}}$.

Figure 9 shows the many-body contributions to ρ at the bcp of O−H and M−O bonds for all aquaions. Due to the different nature of both bonds, their many-body effects for O−H and M−O have different signs: they are negative for the M−O bond, i.e., the intermolecular ionic bond, but $\Delta\rho_{mb}$ is positive for the O−H bond, i.e., the intramolecular covalent bond. An interesting result revealed by this plot is the fact that many-body perturbations are much more important in the ρ(O−H) curves than in the ρ(M−O) ones, as well as its magnitude for the three

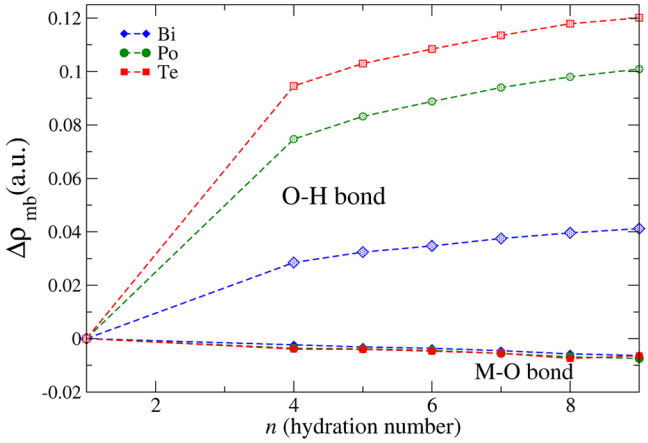

Figure 9. Contribution to the electron density at the M−O and O−H bond critical points due to the many-body effects as a function of the hydration number.

ions, i.e., Te > Po ≫ Bi. The concurrence of the highest charge on Te with its smallest ionic radii helps to understand how its curve presents the extreme behavior, whereas that of Po(IV) remains intermediate with respect to Bi(III) but closer to that of Te.

CONCLUDING REMARKS

In this work, we have carried out a comparative study of the aquaions and hydrolyzed species of Bi(III), Te(IV), and Po(IV) ions in aqueous solutions based on the analysis of structural, bonding, and energetics properties derived from quantum mechanical calculations in the gas phase and in solution. From the energetical point of view, the methodology employed following Scheme 1 is well founded. The error associated with the estimation of the experimental solvation free energy for Bi(III) ion is only 3−4%. For the other two ions, unfortunately, this quantity has not been yet experimentally estimated. ΔG_{sol} computed for Po(IV) and Te(IV) is 700−800 kcal/mol larger than for Bi(III), the Te(IV) value being larger than that of Po(IV) by ∼100 kcal/mol. Most of these differences are justified by the different ion charge and sizes (ion−oxygen distances are shorter for tellurium in all clusters) and by a larger ion−ligand bonding, as shown by QTAIM analysis. The decrease in the solvation number as the hydrolysis degree proceeds, as already observed in the series of Po(IV) hydrolyzed species,[8] has been confirmed for the Te(IV) and Bi(III) cases. It is worth pointing out that in the case of Bi(III) ion, this behavior is exhibited in a steeper way: in all cases the most stable aquaion involves eight to nine water molecules, but only Bi(III) reaches a solvation number equal to 3 for the species involving three hydroxyl groups, Po(IV) and Te(IV) yielding the $[M(H_2O)_3(OH)_3]^+$ species as the most stable one for the same hydrolysis degree. The sequence of most preferred hydrolyzed form shows a common behavior for Te(IV) and Po(IV), against the Bi(III), which exhibits a lesser trend to hydrolyze, agreeing with the experimental hydrolysis equilibria report.[2,18]

Structurally, the three ions present common trends previously observed in Po(IV) ion. However, Te(IV) and Bi(III) ions show a slightly different behavior in some clusters. This is particularly evidenced in the clusters with six ligands such (3,3) and (5,1) species. For the former, the preferred structure in the case of Po(IV) ion can be considered as derived from a regular octahedral distribution. However, in the case of Te(IV) and

dx.doi.org/10.1021/jp309439f | J. Phys. Chem. B 2012, 116, 14903−14914

Bi(III) ions, the optimized arrangement defines a pentagonal pyramidal structure, revealing that even with six ligands, surface clusters can still be observed for these two ions.

The comparative analysis of the bcp for the three ions has revealed that the changes in O−H bond are more sensitive than those occurring in the direct M−O bonds. Many-body effects associated to the aquaions provide a new way to quantify the ion−solvent behavior. The values of ρ(M−O) and ρ(O−H)) on the aquaion series lead to support a larger degree of similarity of Te(IV) with Po(IV) than with Bi(III). When this is added to the preferred hydrolyzed species for the cations and the energetic results lead to conclude that chemical behavior in solution of Po(IV) is closer to that of Te(IV) than to the Bi(III) one. However, this is a first static quantum mechanical approach to a multifaced question that has to be certainly complemented with a dynamical perspective, and with the extension of the research to other oxidation states.

■ ASSOCIATED CONTENT

Supporting Information

Figure of interation energy per water molecule. Table of M−O distances. Tables of Gibbs energy for the successive hydrolysis reactions $[M(H_2O)_n(OH)_m]^{q+} + H_2O \rightarrow [M(H_2O)_n(OH)_m]^{q+} + H_3O^+$ of the three cations. This material is available free of charge via the Internet at http://pubs.acs.org.

■ AUTHOR INFORMATION

Corresponding Author

*E-mail: sanchez@us.es Phone: +34 954557175. Fax: +34 954557174.

Notes

The authors declare no competing financial interest.

■ ACKNOWLEDGMENTS

Spanish DGI of the Ministerio de Economia y Competitividad is acknowledged for financial support (CTQ2011-25932 and MAT2008-06652). Barcelona and CESGA supercomputing centers are acknowledged for the computer time, technical expertise and assistant.

■ REFERENCES

(1) Conway, B. E. *Ionic Hydration in Chemistry and Biophysics. Studies in Physical and Theoretical Chemistry*; Elsevier: Amsterdam, 1981; Vol. *12*.
(2) Baes, C. F., Jr.; Mesmer, R. E. *The Hydration of Cations*; Wiley and Sons: New York, 1976.
(3) Ritchens, D. T. *The Chemistry of Aqua Ions*; Wiley: Chichester, U.K., 1997.
(4) Marcus, Y. *Ion Solvation*; Wiley: Chichester, U.K., 1986.
(5) Ansoborlo, E.; Berard, P.; Auwer, C. D.; Leggett, R.; Menetrier, F.; Younes, A.; Montavon, G.; Moisy, P. *Chem. Res. Toxicol.* **2012**, *25*, 1551−1564.
(6) Matthews, K.; Kim, C.-K.; Martin, P. *Appl. Radiat. Isot.* **2007**, *65*, 267−279.
(7) Ayala, R.; Martínez, J. M.; Pappalardo, R. R.; Muñoz-Páez, A.; Sánchez Marcos, E. *J. Phys. Chem. B* **2008**, *112*, 5416−5422.
(8) Ayala, R.; Martnez, J. M.; Pappalardo, R. R.; Muñoz-Paez, A.; Sánchez Marcos, E. *J. Phys. Chem. B* **2009**, *113*, 487−496.
(9) Ayala, R.; Spezia, R.; Vuilleumier, R.; Martnez, J. M.; Pappalardo, R. R.; Sánchez Marcos, E. *J. Phys. Chem. B* **2010**, *114*, 12866−12874.
(10) Adloff, J.-P.; Kauffman, G. *Chem. Educator* **2007**, *12*, 94−101.
(11) Yang, N.; Sun, H. *Coord. Chem. Rev.* **2007**, *251*, 2354−2366.
(12) Durgai, S.; Hofer, T. S.; Randolf, B. R.; Rode, B. R. *Chem. Phys. Lett.* **2005**, *406*, 20−23.
(13) Pye, C. C.; Gunasekara, C. M.; Rudolph, W. W. *Can. J. Chem.* **2007**, *85*, 945−950.
(14) Kuznetsov, A. M.; Shapnik, M. S.; Masliy, A. N.; Zelenetskaya, K. V. *Russ. J. Electrochem.* **2001**, *38*, 669−675.
(15) Holleman, A. F.; Wiber, E. *Inorganic Chemistry*; Academic Press: Berlin, New York, 2001.
(16) Frank, W.; Reiss, G. J.; Schneider, J. *Angew. Chem. Int. Ed. Engl.* **1995**, *34*, 2416−2417.
(17) Naslund, J.; Persson, I.; Sandstrom, M. *Inorg. Chem.* **2000**, *39*, 4012−4021.
(18) Tytko, K. H. *Chem. Z.* **1979**, *13*, 184−194.
(19) Nabivanets, B. I.; Kapantsyan, E. E. *Russ. J. Inorg. Chem.* **1968**, *13*, 946−949.
(20) Frisch, M. J.; Trucks, G. W.; Schlegel, H. B.; Scuseria, G. E.; Robb, M. A.; Cheeseman, J. R.; Montgomery, J. A., Jr.; Vreven, T.; Kudin, K. N.; Burant, J. C.; et al. *Gaussian 03*, Revision D.01; Gaussian, Inc.: Wallingford, CT, 2004.
(21) Adamo, C.; Barone, V. *J. Chem. Phys.* **1998**, *108*, 664−675.
(22) Dunning, T. H., Jr. *J. Chem. Phys.* **1989**, *90*, 1007−1023.
(23) Metz, B.; Stoll, H.; Dolg, M. *J. Chem. Phys.* **2000**, *113*, 2563−2569.
(24) Peterson, K. A.; Figgen, D.; Goll, E.; Stoll, H.; Dolg, M. *J. Chem. Phys.* **2003**, *119*, 11113−11123.
(25) Peterson, K. A. *J. Chem. Phys.* **2003**, *119*, 11099−11112.
(26) Kerridge, A.; Kaltsoyannis, N. *Chem.—Eur. J.* **2011**, *17*, 5060−5067.
(27) Claverie, P.; Daudey, J. P.; Langlet, J.; Pullman, B.; Piazzola, D.; Huron, M. J. *J. Phys. Chem.* **1978**, *82*, 405−418.
(28) Pappalardo, R. R.; Sánchez Marcos, E.; Rinaldi, D. *J. Phys. Chem.* **1991**, *95*, 8928−8932.
(29) Martínez, J. M.; Pappalardo, R. R.; Sánchez Marcos, E.; Mennucci, B.; Tomasi, J. *J. Phys. Chem. B* **2002**, *106*, 1118−1123.
(30) Tomasi, J.; Persico, M. *Chem. Rev.* **1994**, *94*, 2027−2094.
(31) Tomasi, J.; Mennucci, B.; Cammi, R. *Chem. Rev.* **2005**, *105*, 2999−2993.
(32) Amovilli, C.; Mennucci, B. *J. Phys. Chem. B* **1997**, *101*, 1051−1057.
(33) Mennucci, B.; Martínez, J. M. *J. Phys. Chem. B* **2005**, *109*, 9818−9829.
(34) Zhan, C. G.; Dixon, D. A. *J. Phys. Chem. A* **2004**, *108*, 2020−2029.
(35) Martínez, J. M.; Pappalardo, R. R.; Sánchez Marcos, E. *J. Phys. Chem. A* **1997**, *101*, 4444−4448.
(36) Kelly, P. C.; Cramer, C. J.; Truhlar, D. G. *J. Chem. Theory Comput.* **2005**, *1*, 1133−1152.
(37) Kelly, P. C.; Cramer, C. J.; Truhlar, D. G. *J. Phys. Chem. B* **2006**, *110*, 16066−16081.
(38) Bryantsev, V. S.; Diallo, M. S.; Goddard, W. A., III. *J. Phys. Chem.* **2008**, *112*, 9709−9719.
(39) Bader, R. F. W. *Atoms in Molecules: A quatum Theory*; Oxford University Press: Oxford, U.K., 1990.
(40) Matta, C. F., Boyd, R. J., Eds. *The Quantum Theory of Atoms in Molecules: From Solid State to DNA and Drug Design*; Wiley-UCH: Weinhem, 2007.
(41) Keith, T. A.; T. K. Gristmill, T. K. *AIMALL* (Version 12.06.05); Software: Overland Park, KS, USA, 2012.
(42) Frisch, M. J.; Trucks, G. W.; Schlegel, H. B.; Scuseria, G. E.; Robb, M. A.; Cheeseman, J. R.; Scalmani, G.; Barone, V.; Mennucci, B.; Petersson, G. A.; et al. *Gaussian 09*, Revision C.1; Gaussian, Inc.: Wallingford, CT, 2009.
(43) Keith, T. A.; Frisch, M. J. *J. Phys. Chem. A* **2011**, *115*, 12879−12894.
(44) Greenwood, N. N.; Earnshaw, A. *Chemistry of the Elements*; Butterworth: London, U.K., 1997.
(45) Randaccio, L.; Geremia, S.; Nardin, G.; Wuerges, J. *Coord. Chem. Rev.* **2006**, *250*, 1332−1350.
(46) Kerridge, A.; Kaltsoyannis, N. *Dalton Trans.* **2011**, *40*, 11258−11266.
(47) Marcus, Y. *Chem. Rev.* **1988**, *88*, 1475−1498.

(48) Ohtaki, H.; Radnai, T. *Chem. Rev.* **1993**, *93*, 1157−1204.
(49) Rappe, A. K.; Casewit, C. J.; Colwell, K. S.; Goddard, W. A., III; Skiff, W. M. *J. Am. Chem. Soc.* **1992**, *114*, 10024−10035.